J Biomol NMR (2008) 41:97–104
DOI 10.1007/s10858-008-9245-3

ARTICLE

Double quantum filtering homonuclear MAS NMR correlation spectra: a tool for membrane protein studies

Jakob J. Lopez · Christoph Kaiser · Sarika Shastri · Clemens Glaubitz

Received: 21 February 2008 / Accepted: 27 April 2008 / Published online: 28 May 2008

Abstract ^{13}C homonuclear correlation spectra based on proton driven spin diffusion (PDSD) are becoming increasingly important for obtaining distance constraints from multiply labeled biomolecules by MAS NMR. One particular challenging situation arises when such constraints are to be obtained from spectra with a large natural abundance signal background which causes detrimental diagonal peak intensities. They obscure cross peaks, and furthermore impede the calculation of a buildup rates matrix which may be used to derive distance constraints, as carried out in "NMR crystallography". Here, we combine double quantum (DQ) filtering with ^{13}C–^{13}C dipolar assisted rotational resonance (DARR) experiments to yield correlation spectra free of natural abundance contributions. Two experimental schemes, using DQ filtering prior to evolution (DOPE), and after mixing (DOAM), have been evaluated. Diagonal peak intensities along the spectrum diagonal are removed completely, and crosspeaks close to the diagonal are easily identifiable. For DOAM spectra with negligible mixing times, it is possible to carry out 'assignment walks' which simplify peak identification substantially. The method is demonstrated on ^{13}C-cys labeled proteorhodopsin, a 27 kDa membrane protein. The magnetization transfer characteristics were studied using buildup curves obtained on uniformly ^{13}C labelled crystalline tripeptide MLF. Our data show that DQ filtered DARR experiments pave the way for obtaining through space constraints for structural studies on ligands, bound to membrane receptors, or on small fragments within large proteins.

Keywords Solid state NMR · MAS NMR · Double quantum filtering · Homonuclear correlation · PDSD · DARR

Abbreviations

PDSD	Proton driven spin diffusion
DARR	Dipolar assisted rotational resonance
NMR	Nuclear magnetic resonance
MAS	Magic angle spinning
DQF	Double quantum filtering
DOPE	Double quantum filtering prior to evolution
DOAM	Double quantum filtering after mixing
NA	Natural abundance
PR	Proteorhodopsin

Introduction

Solid-state NMR (ssNMR) is becoming an increasingly important method for obtaining structural data from biomolecules. In particular, homonuclear correlation techniques such as ^{13}C–^{13}C proton driven spin diffusion (PDSD) (Szeverenyi et al. 1982), dipolar assisted rotational resonance (DARR) (Takegoshi et al. 2001) or CHHC polarization transfer experiments (Lange et al. 2002), together with uniform isotope labeling of proteins, allow a large number of distance constraints to be obtained simultaneously. For established

Jakob J. Lopez and Christoph Kaiser—contributed equally to this work.

Electronic supplementary material The online version of this article (doi:10.1007/s10858-008-9245-3) contains supplementary material, which is available to authorized users.

J. J. Lopez · C. Kaiser · S. Shastri · C. Glaubitz (✉)
Institute for Biophysical Chemistry, Centre for Biomolecular Magnetic Resonance, J. W. Goethe University Frankfurt, Max-von-Laue-Str. 9, 60438 Frankfurt, Germany
e-mail: glaubitz@em.uni-frankfurt.de

liquid state NMR protocols and the case of the more recent "NMR crystallography" (Elena and Emsley 2005; Elena et al. 2006; Pickard et al. 2007), such constraints are important for macromolecular structure calculations of high resolution. However, the situation becomes rather challenging when such spectra are acquired on small, uniformly labeled molecules embedded into protein/lipid complexes, which are the source of large ^{13}C natural abundance (NA) background signals. Such a situation is typically encountered, for example, with uniformly ^{13}C labeled neuropeptides bound to GPCRs (Lopez et al. 2008; Luca et al. 2003), or single ^{13}C labeled amino acids within large membrane proteins (Lehner et al. 2008). The difficulty here lies in the fact that signals from the labeled compounds are obscured by the large natural abundance (NA) peak intensities along the DARR spectrum diagonal, which is typically larger in intensity by several orders of magnitude.

In the past, ^{13}C isotope labeling has sufficed for the structural investigation of membrane proteins in reconstituted form (Creemers et al. 2002; Creuzet et al. 1991; Guo et al. 1996) or peptide/protein complexes (Weliky et al. 1999). For these examples, the ratio of the signals which stem from labeled sample (S_L) and the natural abundance (NA) background (S_{NA}) proves to be $S_L/S_{NA} \sim 10^{-2}$, which is sufficient for ssNMR experiments on protein systems. However, for the case of samples involving large membrane protein/lipid complexes, S_L/S_{NA} becomes much smaller, and the signal of the ligand, although labeled, is obscured by the signal background from NA ^{13}C nuclei found in the membrane protein and its reconstitution environment (detergent micelles or lipid membranes). Here, DQ filtering (Bax et al. 1980; Munowitz and Pines 1986, 1987; Munowitz et al. 1987) has proven to be the crucial step: past ssNMR studies of ligands bound to reconstituted membrane protein receptors were possible only because DQ filtering causes the signals of isolated ^{13}C nuclei to be removed from the NA background spectrum. This lowers the ratio S_L/S_{NA} at which ssNMR experiments may be carried out, roughly by two orders of magnitude ($S_L/S_{NA} \sim 10^{-4}$ (Luca et al. 2003)). A solution to this problem are DQ filtered experiments with which chemical shift values of GPCR bound neuropeptides, for example, have lead to backbone structures (Lopez et al. 2008; Luca et al. 2003), or the characterization of single aminoacids within multidrug transporters (Lehner et al. 2008). The DQSQ experiments used in these examples yield protein backbone torsion angle constraints via chemical shift values. DARR experiments are complementary and deliver through space constraints via dipolar couplings which are represented through relative cross peak intensities and buildup rates. Whilst DQSQ experiments are inherently suited for samples with a high NA ^{13}C background, DARR pulse sequences with DQ filtering are currently not obtainable within the repertoire of existing ssNMR techniques, a fact which has motivated the work reported in this communication.

Here, we describe DARR experiments (Takegoshi et al. 2001) which are extended by pulse sequence blocks and phase cycling in which DQ coherence is first excited and then reconverted to single quantum coherences. Two schemes for DQ filtering DARR experiments are depicted in Fig. 1. In the first (Fig. 1a), DQ filtering occurs after Hartman–Hahn ^{1}H-X magnetization transfer, before chemical shift evolution. In the second (Fig. 1b), DQ filtering is achieved after longitudinal magnetization exchange for a period t_{mix}, before signal acquisition. For convenience, in the remainder of this publication, we will make use of the abbreviations DOPE (*Do*uble Quantum Filtering *P*rior to *E*volution) and DOAM (*Do*uble Quantum Filtering *A*fter *M*ixing) to distinguish between the two strategies.

The pulse sequences we introduce here are developed with structural studies of GPCR bound ligands in mind (Lopez et al. 2008; Luca et al. 2003). GPCRs, reconstituted, in a lipid medium, and complexed with a natural

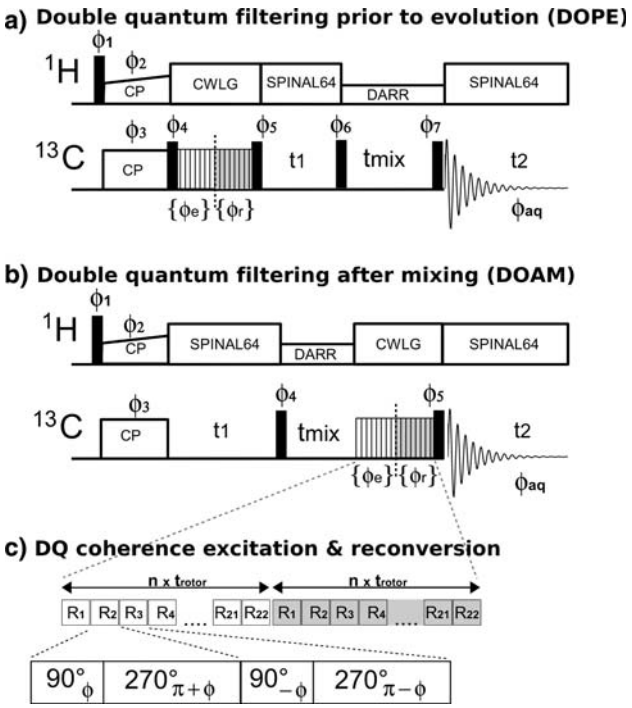

Fig. 1 DQ filtering schemes for DARR experiments. DQ filtering prior to evolution (DOPE, upper scheme) is achieved before the chemical shift evolution by excitation of magnetization due to DQ coherences, and its immediate rerouting to SQ coherence pathways. For DQ filtering after mixing (DOAM, middle scheme), the DQ excitation-reconversion block is placed at the end of the DARR pulse sequence. $R22_4^9$ is schematically depicted (lowest scheme), the phases of the R sequences have collectively been summed up in (a) and (b), for DQ excitation $\{\phi_e\}$ and DQ reconversion (shaded) $\{\phi_r\}$, in order to describe their super cycling for DQ filtering by phase cycling (see text)

ligand, require a large amount of care and effort. For this communication, we refrain from using such mammalian membrane proteins. Instead, our study involves (i) testing DQ filtered DARR sequences on the reconstituted bacterial transmembrane photoreceptor proteorhodopsin (PR, 27 kDa) of which three cysteine residues are uniformly ^{13}C labeled, and (ii) comparing the effect of DQ excitation and reconversion on crosspeak intensities in the DARR, DOPE and DOAM spectra of the tripeptide MLF, for different mixing times. We describe the experimental details and the results in the following pages.

Materials and methods

NMR pulse sequences

In the following, we describe DARR experiments (Takegoshi et al. 2001) which are extended by pulse sequence elements designed to first excite DQ coherences and then subsequently reconvert them to single quantum coherences.

Symmetry theorems for MAS NMR experiments during which radiofrequency (rf) pulses are timed to coincide with the MAS rotor revolutions allow the NMR spectroscopist to tailor the Hamiltonian under which the magnetization evolves (Levitt 2008). Here, for DQ filtering, the symmetry-derived pulse sequence block $SR22_4^9$ is incorporated into the experiment. This block belongs to a class of sequences which may be described with the shorthand notation SRN_n^v (Carravetta et al. 2001), where R denotes an element in which the resonant spins are rotated about the x-axis (of the rotating frame) through the angle π. A second element R′ follows, which is identical to its predecessor R, but with an rf pulse phase of opposing sign (see Fig. 1c). The properties of this particular sequence block ($N = 22$, $v = 9$, $n = 4$) lead to a γ-encoded CSA-compensated dipolar recoupling between X nuclei (Carravetta et al. 2001). Of course, other established DQ coherence recoupling sequences, such as for example PC7 (Carravetta et al. 2000) and SPC5 (Hohwy et al. 1999) are expected to give comparable results.

For the case of DQ filtering before the chemical shift evolution (Fig. 1a, DOPE), bracketing pulses are placed on either side of the array of R-elements, in order to create longitudinal magnetization before the DQ filtering, and transverse magnetization after the DQ excitation/reconversion, for the ensuing chemical shift evolution (of duration t_1).

For the case of DQ filtering after magnetization exchange (Fig. 1b, DOAM), bracketing pulses are unnecessary: longitudinal magnetization is already present before filtering, and is converted to transverse magnetization by the readout pulse, for signal acquisition.

To avoid interference by a Hartman–Hahn transfer during DQ excitation and reconversion, we have subdued any ^1H–^{13}C magnetization transfer by applying homonuclear Lee–Goldburg (Lee and Goldburg 1965; Vinogradov et al. 1999) decoupling during DQ excitation and reconversion in both, DOPE and DOAM experiments.

Setup and parameter values

NMR experiments were conducted using two widebore Bruker Avance spectrometers (Bruker Biospin, Karlsruhe, Germany), respectively operating at ^1H frequencies of 400 MHz and 600 MHz, each equipped with a triple-resonance (^1H, ^{13}C, ^{15}N) MAS DVT probe head (4 mm rotor diameter).

Experimental parameters were very similar for all experiments, and are listed respectively in the following, for the 400 MHz and 600 MHz (in brackets) spectrometers: for Hartmann–Hahn ^1H to ^{13}C cross-polarization (Hartmann and Hahn 1962), the contact pulse duration is 1,000 μs (750 μs), ^1H spinlock power levels were ramped from 80% to 100%: 46 kHz (62 kHz), with ^{13}C spinlock power levels of 44 kHz (44 kHz), and $\pi/2$ pulse lengths for ^1H: 4.25 μs (3 μs), $\pi/2$ pulse lengths for ^{13}C: 4.55 μs (4 μs). SPINAL64 decoupling (Fung et al. 2000) was used during chemical shift evolution and signal acquisition, at a power level of 74 kHz (83 kHz).

DQ excitation and recoupling were achieved with the symmetry derived pulse sequence block $SR22_4^9$, with equal DQ excitation and SQ reconversion times of 410 μs (500 μs). Lee Goldburg decoupling was set up on adamantane, by varying the ^1H r.f. field strength for a given pulse length until ^1H–^{13}C J-couplings could be resolved. Here, an effective ^1H decoupling field of $B1/\sqrt{2} = 66$ kHz (83 kHz) was used.

On PR, 2D DARR spectra and the DQ filtered versions thereof were acquired with 2048 (F2) points and 128 (F1) increments (1024 scans per increment).

Magnetization buildup curves (Fig. 3) were obtained on U-^{13}C-MLF by acquiring 2D ^{13}C MAS—DARR, DOPE and DOAM (Fig. 4) spectra at mixing times of (in seconds): 0.001, 0.005, 0.010, 0.025, 0.050, 0.100, 0.150, and 0.200 per increment. Here, spectra were acquired with 1024 points, 128 increments and 64 acquisitions. All 2D experiments were carried out with phase sensitive detection (TPPI) at an MAS speed of 10 kHz, with a recycle delay time of 2 s, at a temperature of 290 K.

Phasecycling

In order to ensure that only coherences generated by Hartman Hahn $^1H \rightarrow {}^{13}C$ magnetization transfer are propagated during the experiment, ϕ_1 and ϕ_{aq} are synchronously alternated between y and −y for each acquisition.

Table 1 Phase cycling for DOPE (a) and DOAM (b) pulse sequences. Denoted in bold are the phasecycles used to filter any coherences which do not travel along double quantum coherence pathways

(a) DOPE

ϕ_1	ϕ_2	ϕ_3	ϕ_4	$\{\phi_r\}$	ϕ_5	ϕ_6	ϕ_7	ϕ_{aq}
y	y	x	−x	**y**	**y**	**−y**	x	x
y	y	x	−x	**−x**	**−x**	**−x**	x	x
y	y	x	−x	**−y**	**−y**	**y**	x	x
y	y	x	−x	**x**	**x**	**x**	x	x
−y	y	x	−x	**y**	**y**	**−y**	x	−x
−y	y	x	−x	**−x**	**−x**	**−x**	x	−x
−y	y	x	−x	**−y**	**−y**	**y**	x	−x
−y	y	x	−x	**x**	**x**	**x**	x	−x

(b) DOAM

ϕ_1	ϕ_2	ϕ_3	ϕ_4	$\{\phi_r\}$	ϕ_5	ϕ_{aq}
y	y	x	x	**y**	**y**	**−y**
y	y	x	x	**−x**	**−x**	**−x**
y	y	x	x	**−y**	**−y**	**y**
y	y	x	x	**x**	**x**	**x**
−y	y	x	x	**y**	**y**	**y**
−y	y	x	x	**−x**	**−x**	**x**
−y	y	x	x	**−y**	**−y**	**−y**
−y	y	x	x	**x**	**x**	**−x**

DQ filtering is achieved by conventional phasecycling, in which the phases of two pulse sequence blocks are cycled in a concerted manner with respect to each other (Bodenhausen et al. 1984).

For both DOPE and DOAM experiments, the array of R elements which reconvert DQ coherence to SQ coherence (phases $\{\phi_r\}$ in Fig. 1, shaded elements), together with the second bracket pulse (phase ϕ_5), constitute the first entity to be phasecycled. Their phases are incremented by 90° with each acquisition.

In order to filter out any magnetization not due to DQ coherence pathways, the pulse positioned at the end of the chemical shift evolution (DOPE, Fig. 1a, ϕ_6) and the receiver phase (DOAM, Fig. 1b, ϕ_{aq}) were cycled according to {−y −x y x}. Conclusively, the final phase cycles used in the experiments consists of eight steps, and are listed in Table 1a (DOPE) and b (DOAM).

Processing, analysis and plotting

If not mentioned otherwise in the figure captions, all spectra were processed by doubling the number of points in each dimension, using 'zero filling'. Automatic baseline corrections and window functions were applied in the direct (exponential form, 50 Hz) and indirect dimension ("squared sine" function, with a sine bell shift of π/2, corresponding to a pure cosine function).

All experimental data were processed with TopSpin 2.0 (Bruker BioSpin, Karlsruhe, Germany). Peak picking and integration was carried out with the help of the software package Cara 1.8.3 (Keller et al. 2006). Plotting and data analysis was carried out with the help of scripts written in house, using Python 2.5 (http://www.python.org), more specifically with the library of mathematical functions which are supplied in the python modules 'pylab' (http://matplotlib.sourceforge.net) and 'SciPy' (http://www.scipy.org, (Jones et al. 2002)). With the exception of TopSpin, all software is available for download on the world wide web, at no cost.

Data Analysis: Buildup curves (see Fig. 3) were calculated with the "full matrix rate analysis," (Huster et al. 1999). In short, experimentally measured DARR peak volumes, represented by matrix **A**, at the mixing time t_m, and the cross-relaxation rate matrix **R** are linked by the following matrix equation.

$$\mathbf{A}(t_m) = \mathbf{A}(0) \cdot \exp(-\mathbf{R}t_m) \quad (1)$$

The relaxation rate matrix R is calculated by rewriting Eq. 1 as follows.

$$\mathbf{R} = -\frac{\mathbf{X}(\ln \mathbf{D})\mathbf{X}^{-1}}{t_m}$$

Here, **X** is the matrix of eigenvectors, and **D** is the diagonal matrix of eigenvalues of the normalized peak volume matrix $a(t_m) = \mathbf{A}(t_m)[(\mathbf{A}(0)^{-1}]$.

Sample preparation

Two samples were used for NMR measurements: First, the integral membrane protein proteorhodopsin (PR, 27 kDa), reconstituted into DOPC in 2D crystalline form, with selectively ^{13}C labeled cysteines which are found at positions 107, 156 and 175 (see Fig. 2, inset). Second, the chemotactic tripeptide MLF, uniformly ^{13}C and ^{15}N labelled.

The expression of wild type PR was essentially carried out as described in (Shastri et al. 2007). In short, the cells were grown in defined medium with 50 μg/ml Kanamycin until the optical density reached 0.8. The cells were then resuspended in a freshly mixed medium with labeled cysteine (50 mg/l). One mM IPTG (isopropyl-beta-D-thiogalactopyranoside) was used for induction along with 0.7 mM all-trans retinal dissolved in ethanol for PR over-expression. Cells were harvested after 4 h of incubation at 37°C. The harvested cells were broken open using a cell disruptor, and the membrane fraction was obtained after ultracentrifugation. The membranes were solubilized in 1.5% DDM. Detergent solubilised histidine tagged protein was purified using a Ni-NTA (nitrilo-triacetic acid) column and eluted in 0.2% Triton X. The concentration of protein was estimated

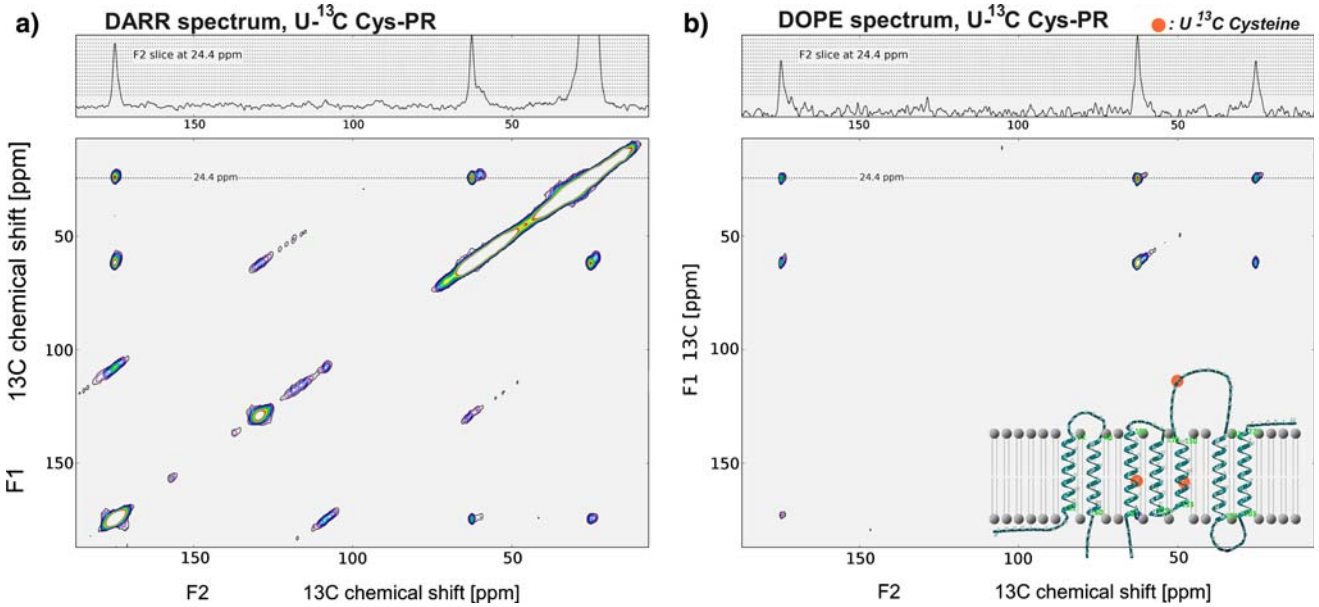

Fig. 2 DARR and DOPE spectra on reconstituted PR, with selectively ^{13}C labeled cysteines 107, 156 and 175 (marked by orange circles on the protein, see inset picture). For both DARR and DOPE spectra, 16 equidistant contour levels were chosen, with a minimum value just above the baseline, and a maximum value corresponding to the crosspeak intensity at 67.7 and 24.4 ppm (see slices, at top). The diagonal intensity is the dominant spectrum characteristic in the conventional DARR spectrum, along with MAS spinning sidebands, and is completely removed in the DOPE spectrum. Any background contribution from ^{13}C NA intensities, stemming from the large membrane protein and its reconstitution environment (lipid bilayer), is removed

using UV-vis spectroscopy, and adjusted to 1 mg/ml. Appropriate lipids (DOPC, 1,2-Dioleoyl-*sn*-Glycero-3-phosphocholine) were added just prior to setting up the 2D crystalline preparation by means of dialysis for 1 week with regular buffer changes. The crystalline sample was finally pelleted and transferred to a 4 mm MAS rotor. For the measurements, the rotor contained $\sim$15 mg of the sample.

Formyl-[U-^{13}C,^{15} N]-Met-Leu-Phe-OH (MLF) was purchased from euriso-top GmbH, Saarbrücken, Germany, and used without further purification. 3 mg of the peptide were transferred to a 4 mm MAS rotor for measurement.

Results and discussion

In the following, we show the efficacy of DQ filtering a DARR spectrum. Furthermore, we discuss the effect of DQ filtering on the cross peak intensities and buildup rates by comparing experimental buildup curves of DARR, DOPE and DOAM experiments, and demonstrate assignment walks obtained with DOAM experiments.

DQ-filtering: spectrum simplification by removal of natural abundance background signals

DARR, DOPE and DOAM spectra were acquired with the membrane protein PR, containing three uniformly ^{13}C labeled cysteines (Fig. 2b, inset). In Fig. 2, DARR and DOPE spectra are depicted side by side (DOAM not pictured). To facilitate the comparison, contour levels are adjusted to cover, from top to bottom, the cross peak found at 67.7, 24.4 ppm (see inset of 1D slice, at top) for both contour plots.

In the DARR spectrum, NA ^{13}C nuclei occurring in the membrane protein and in its membrane reconstitution environment are the source of diagonal peak intensities which are more than a magnitude larger than that of the crosspeak at 62.7 and 24.4 ppm (see Fig. 2). It is worth mentioning that, for other membrane proteins (GPCRs), this factor is in general much higher (100–1000:1), causing diagonal peak intensities several magnitudes larger.

For the purpose of demonstrating the efficacy of the DQ filtering schemes presented here, the results are clear: the DOPE spectrum features peaks stemming only from the ^{13}C labeled cysteines, the diagonal peak intensities due to ^{13}C NA contributions are completely removed.

It is worth noting that, due to the addition of the DQ filter, the sensitivity of a DOPE or DOAM experiment is reduced in comparison to a DARR spectrum. The DQ filtered experiments yield 40% of the DARR signal strength, and result in a lower signal to noise ratio, as observable on comparing the 1D spectrum slices at the tops of Fig. 2a and b.

Intensities

In ssNMR spectroscopy, a large number of spatial constraints between sites in a protein can be obtained by the

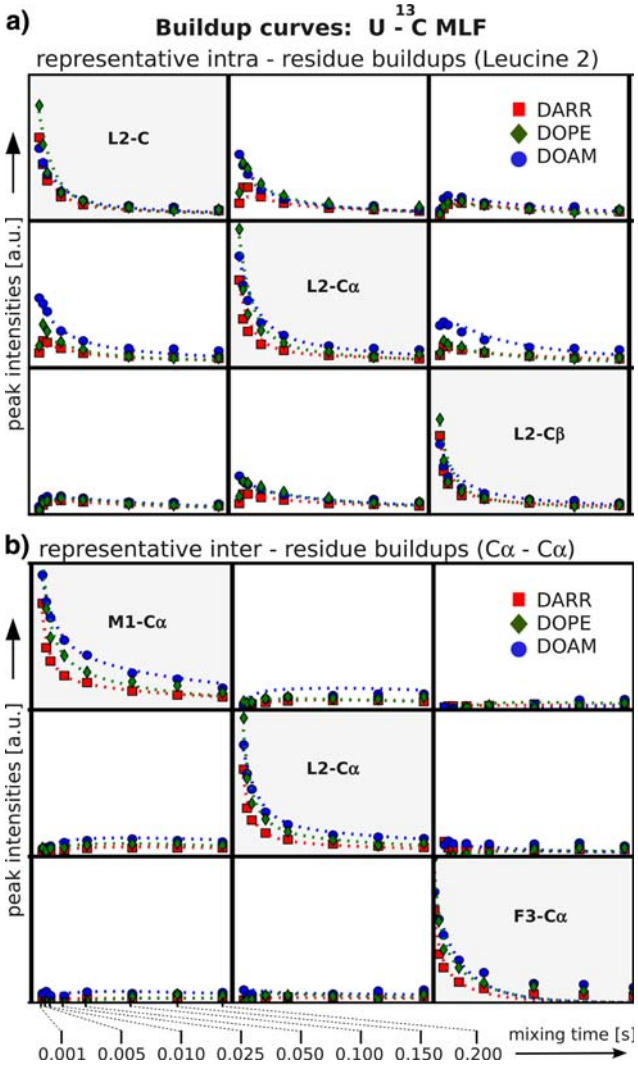

Fig. 3 A comparison of relative crosspeak intensities of uniformly ^{13}C labelled MLF for DARR, DOPE and DOAM experiments. For clarity, we focus on intra-residue build-ups within Leu-2 (above, **a**), and the inter-residue build-ups between Cα atoms (below, **b**). Dotted lines are the result of curves calculated with magnetization rates that were obtained by fitting with the full matrix approach (see materials and methods), and are intended to guide the eye. The intensity curves are plotted over mixing times. In the initial buildup regime, the intensities of the curves are identical. Buildup rates were unaffected by the addition of DQ filtering pulse elements to the DARR sequence. Spectra were acquired with uniformly ^{13}C labelled MLF

acquisition of a single DARR spectrum. In such homonuclear correlation experiments, the cross peak intensities of nuclear pairs are measured at certain mixing times, and subsequently used to estimate distances between nuclear sites.

With the introduction of a DQ filter into the DARR experiment, it is necessary to ensure that cross peak intensities can still be used to obtain internuclear distance constraints as shown for PDSD or DARR experiments without DQ filtering. Intensity modulation from DQ buildup curves have been used for precise internuclear distance measurements (Carravetta et al. 2001). In DOPE or DOAM experiments, such intensity changes, manifesting themselves through modulations of cross peak intensities over the course of several mixing periods, would undermine the proportionality between crosspeak intensity and internuclear distance. To ensure that DQ filtering of DARR experiments does not affect the relative intensities between crosspeaks, DARR, DOPE and DOAM spectra were acquired for a range of different mixing times. Measurements were carried out on the chemotactic tripeptide MLF, a sample which has been thoroughly studied with ssNMR (Hong et al. 1997; Rienstra et al. 2002), and which lends itself well as a standard, due to highly resolved ^{13}C spectra.

As depicted in Fig. 3, the typical exponential decay of the diagonal peaks, and magnetization buildup and decay of the cross peaks, is readily discernible for DARR, DOPE and DOAM experiments acquired over a range of mixing times. For the sake of clarity we focus, in Fig. 3a, on the diagonal- and cross peaks of the backbone carbons C, Cα and Cβ of the center amino acid leucine and, in Fig. 3b, on the Cα—Cα crosspeak intensities of the peptide backbone. As is evident from the plot, for both, intra-residue (one- to two-bond) and inter-residue distances, the relative intensities of the crosspeaks are unaffected by the addition of the DQ filtering blocks, for both DOPE and DOAM.

For the case of DARR and DOPE experiments, the relative crosspeak intensities remain comparable. For DOAM, however, this is only the case for nuclei which are not directly bonded. Crosspeaks belonging to the neighbouring nuclear pairs of C′–Cα and Cα–Cβ exhibit their highest signal intensity at the beginning of the buildup curves (see Fig. 3a), due to a magnetization transfer facilitated by the dipolar recoupling of the bonded pairs by the DQ excitation which is achieved during $SR22_4^9$ dipolar excitation.

Buildup rates

Spatial constraints for protein structure calculations can be derived from cross peak buildup curves, as described above for cross peak intensities. It is necessary to ensure that cross peak buildup rates are also not affected by the excitation of DQ coherences during the acquisition of DARR spectra. A comparison of the rates with which the intensities grow before reaching their maximum shows matching buildup curves for the DARR and DOPE experiments (plots see supplementary material). DOAM experimental buildup curves, however, need to be divided into two classes: The profile of DOAM buildup curves for nuclear pairs which are nonbonded exhibits rates which are comparable to those of DARR and DOPE experiments (see

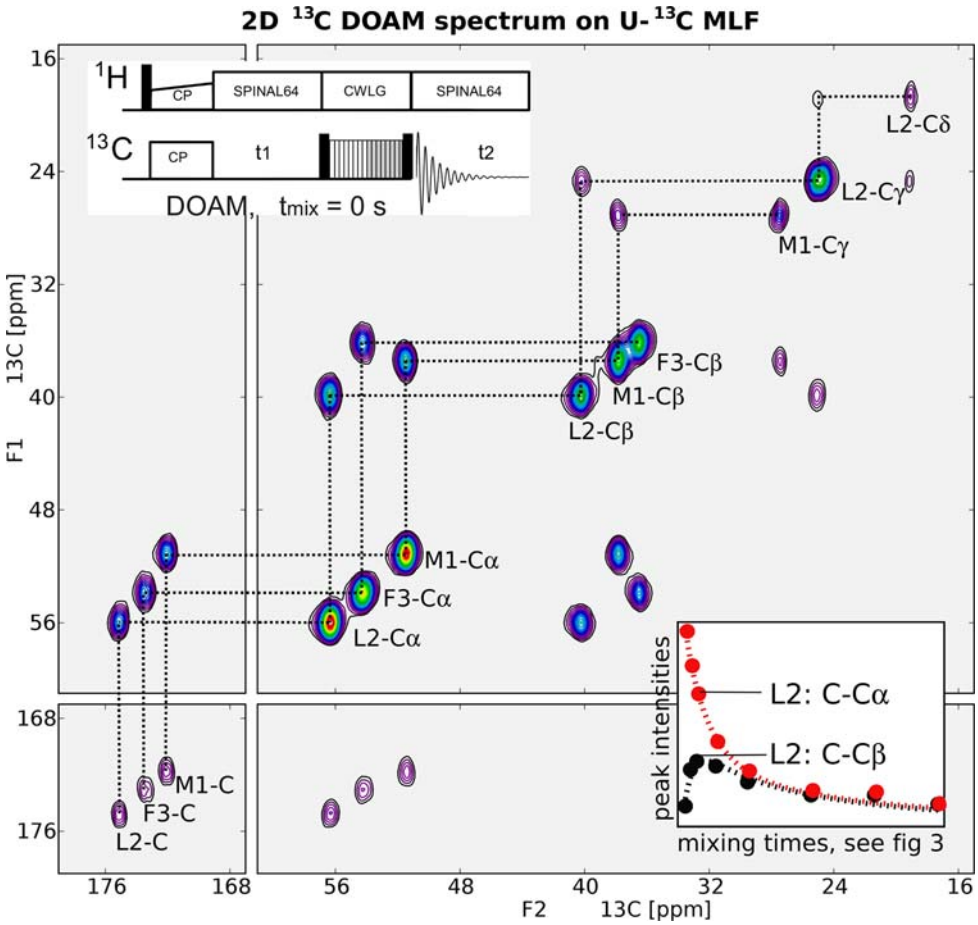

Fig. 4 DOAM spectrum of uniformly ^{13}C labeled MLF, with a mixing time of zero. Assignment walks are indicated by horizontal and vertical dotted lines. Crosspeaks are visible only for directly neighbouring (bonded) nuclei. This is not an effect of choosing appropriate contour levels. At this negligible mixing time, crosspeaks are due only to dipolar coupling between adjacent nuclei. Crosspeak intensities for nonbonded nuclei exhibit negligible intensities for short mixing times (see picture inset)

Fig. 3b). Buildup curves of neighboring nuclei, directly bonded, exhibit a maximum at the beginning of the mixing time, and decay in an exponential manner.

DOAM: assignment walks

As described above, DOAM cross peak intensities for neighboring nuclei have their maxima at the beginning of the intensity buildup curves. As a consequence, the acquisition of 2D DOAM spectra at $t_{mix} = 0$ s (see inset schematic of the pulse sequence at the top of Fig. 4) leads to homonuclear correlation spectra which exhibit cross-peaks only from coupled nuclei. As indicated in Fig. 4, this leads to the possibility of performing 'assignment walks', which can simplify the identification and assignment of peaks substantially.

Summary and conclusion

The experiments introduced in this communication fulfill the need for DQ filtered homonuclear correlation spectra in the ssNMR biomembrane toolbox. Of very high interest currently are the interactions between molecules in native lipid membrane systems. Unfortunately, this highly relevant class of samples intrinsically involves a high ^{13}C natural abundance background, due to the lipid bilayer and the size of the membrane proteins, and currently limits the application of ssNMR experiments severely.

A typical example is a recent ssNMR study which delivers compelling experimental evidence that the protonation state of a GPCR-bound agonist (Histamine) is able to influence receptor activation (Ratnala et al. 2007). In this important study, the identification of histidine resonances within a PDSD spectrum was obtained by conducting an additional DQ filtered experiment. The pulse sequences introduced here obviate the need for such additional experiments, and deliver the same information within one experiment.

The DOPE and DOAM experiments introduced here allow the identification, assignment and the gathering of spatial information, without being impeded by a large amount of ^{13}C nuclei due to NA. DOPE experiments yield relative cross peak intensities and buildup rates which are unaffected by DQ filtering, as indicated by a comparison to DARR spectra under identical conditions.

It is predictable that, of the two possibilities, DOPE will be the more routine experiment when it comes to gathering information concerning structural constraints. DOAM

experiments yield buildup curves which may be split into two classes, depending on whether they are from peaks from bound or nonbound nuclei. Crosspeak intensities originating from bound nuclei are characterized by a maximum intensity for a mixing time of $t_{mix} = 0$ s, and may mostly be useful in the identification and assignment of amino acid backbone crosspeaks, on assignment walks based on the knowledge of the backbone structure.

Acknowledgements Support by the Center of Biomolecular NMR and the European Union (EU-NMR) is acknowledged.

References

Bax A, Freeman R, Kempsell SP (1980) Natural abundance C-13–C-13 coupling observed via double-quantum coherence. J Am Chem Soc 102:4849–4851

Bodenhausen G, Kogler H, Ernst RR (1984) Selection of coherence-transfer pathways in NMR pulse experiments. J Magn Reson 58:370–388

Carravetta M, Eden M, Zhao X, Brinkmann A, Levitt MH (2000) Symmetry principles for the design of radiofrequency pulse sequences in the nuclear magnetic resonance of rotating solids. Chem Phys Lett 321:205–215

Carravetta M, Eden M, Johannessen OG, Luthman H, Verdegem PJE, Lugtenburg J, Sebald A, Levitt MH (2001) Estimation of carbon–carbon bond lengths and medium-range internuclear: distances by solid-state nuclear magnetic resonance. J Am Chem Soc 123:10628–10638

Creemers AFL, Kiihne S, Bovee-Geurts PHM, DeGrip WJ, Lugtenburg J, de Groot HJM (2002) H-1 and C-13 MAS NMR evidence for pronounced ligand–protein interactions involving the ionone ring of the retinylidene chromophore in rhodopsin. Proc Natl Acad Sci U S A 99:9101–9106

Creuzet F, Mcdermott A, Gebhard R, Vanderhoef K, Spijkerassink MB, Herzfeld J, Lugtenburg J, Levitt MH, Griffin RG (1991) Determination of membrane-protein structure by rotational resonance NMR—bacteriorhodopsin. Science 251:783–786

Elena B, Emsley L (2005) Powder crystallography by proton solid-state NMR spectroscopy. J Am Chem Soc 127:9140–9146

Elena B, Pintacuda G, Mifsud N, Emsley L (2006) Molecular structure determination in powders by NMR crystallography from proton spin diffusion. J Am Chem Soc 128:9555–9560

Fung BM, Khitrin AK, Ermolaev K (2000) An improved broadband decoupling sequence for liquid crystals and solids. J Magn Reson 142:97–101

Guo W, Groesbeek M, Salmon A, Smith SO, Hamilton JA (1996) Characterization of phospholipid crystals by magic angle spinning (MAS) NMR. Biophys J 70:Su326–Su326

Hartmann SR, Hahn EL (1962) Nuclear double resonance in the rotating frame. Phys Rev 128:2042–2053

Hohwy M, Rienstra CM, Jaroniec CP, Griffin RG (1999) Fivefold symmetric homonuclear dipolar recoupling in rotating solids: application to double quantum spectroscopy. J Chem Phys 110:7983–7992

Hong M, Gross JD, Rienstra CM, Griffin RG, Kumashiro KK, Schmidt-Rohr K (1997) Coupling amplification in 2D MAS NMR and its application to torsion angle determination in peptides. J Magn Reson 129:85–92

Huster D, Arnold K, Gawrisch K (1999) Investigation of lipid organization in biological membranes by two-dimensional nuclear overhauser enhancement spectroscopy. J Phys Chem B 103:243–251

Jones E, Oliphant T, Peterson P (2002) SciPy: open source scientific tools for Python. http://www.scipy.org

Keller R, Grace CRR, Riek R (2006) Fast multidimensional NMR spectroscopy by spin-state selective off-resonance decoupling (SITAR). Magn Reson Chem 44:S196–S205

Lange A, Luca S, Baldus M (2002) Structural constraints from proton-mediated rare-spin correlation spectroscopy in rotating solids. J Am Chem Soc 124:9704–9705

Lee M, Goldburg WI (1965) Nuclear-magnetic-resonance line narrowing by a rotating Rf field. Phys Rev 140:1261–1269

Lehner I, Basting D, Meyer B, Haase W, Manolikas T, Kaiser C, Karas M, Glaubitz C (2008) The key residue for substrate transport (Glu14) in the EmrE dimer is asymmetric. J Biol Chem 283:3281–3288

Levitt MH (2008) Symmetry in the design of NMR multiple-pulse sequences. J Chem Phys 128:052205

Lopez JJ, Shukla AK, Reinhart C, Schwalbe H, Michel H, Glaubitz C (2008) The structure of the neuropeptide bradykinin bound to the human G-protein coupled receptor bradykinin B2 as determined by solid-state NMR spectroscopy. Angew Chem Int Ed Engl 47:1668–1671

Luca S, White JF, Sohal AK, Filippov DV, van Boom JH, Grisshammer R, Baldus M (2003) The conformation of neurotensin bound to its G protein-coupled receptor. Proc Natl Acad Sci U S A 100:10706–10711

Munowitz M, Pines A (1986) Multiple-quantum nuclear-magnetic-resonance spectroscopy. Science 233:525–531

Munowitz M, Pines A (1987) Principles and applications of multiple-quantum NMR. Adv Chem Phys 66:1–152

Munowitz M, Pines A, Mehring M (1987) Multiple-quantum dynamics in NMR—a directed walk through Liouville space. J Chem Phys 86:3172–3182

Pickard CJ, Salager E, Pintacuda G, Elena B, Emsley L (2007) Resolving structures from powders by NMR crystallography using combined proton spin diffusion and plane wave DFT calculations. J Am Chem Soc 129:8932–8933

Ratnala VR, Kiihne SR, Buda F, Leurs R, de Groot HJ, DeGrip WJ (2007) Solid-state NMR evidence for a protonation switch in the binding pocket of the H1 receptor upon binding of the agonist histamine. J Am Chem Soc 129:867–872

Rienstra CM, Tucker-Kellogg L, Jaroniec CP, Hohwy M, Reif B, McMahon MT, Tidor B, Lozano-Perez T, Griffin RG (2002) De novo determination of peptide structure with solid-state magic-angle spinning NMR spectroscopy. Proc Natl Acad Sci U S A 99:10260–10265

Shastri S, Vonck J, Pfleger N, Haase W, Kuehlbrandt W, Glaubitz C (2007) Proteorhodopsin: characterisation of 2D crystals by electron microscopy and solid state NMR. Biochim Biophys Acta 1768:3012–3019

Szeverenyi NM, Sullivan MJ, Maciel GE (1982) Observation of spin exchange by two-dimensional Fourier-transform C-13 cross polarization-magic-angle spinning. J Magn Reson 47:462–475

Takegoshi K, Nakamura S, Terao T (2001) C-13-H-1 dipolar-assisted rotational resonance in magic-angle spinning NMR. Chem Phys Lett 344:631–637

Vinogradov E, Madhu PK, Vega S (1999) High-resolution proton solid-state NMR spectroscopy by phase-modulated Lee-Goldburg experiment. Chem Phys Lett 314:443–450

Weliky DP, Bennett AE, Zvi A, Anglister J, Steinbach PJ, Tycko R (1999) Solid-state NMR evidence for an antibody-dependent conformation of the V3 loop of HIV-1 gp120. Nat Struct Biol 6:141–145